Rev. Roum. Sci. Techn.– Électrotechn. et Énerg.
Vol. **70**, *1*, pp. 3–8, Bucarest, 2025

A NOVEL DESIGN OF A PHOTOVOLTAIC SYSTEM BASED ON A LINEAR INDUCTION MOTOR AND RECIPROCATING PUMP

LAID KHETTACHE[1], MOHAMED REDHA REZOUG[1], AKRAM SAADI[2], LAZHAR SAHRAOUI[1]

Keywords: Photovoltaic; Linear induction motor; Reciprocating pump; Field-oriented control; Maximum power point.

This paper presents a novel approach to enhance the efficiency and performance of photovoltaic (PV)-water pumping systems by integrating a linear induction motor (LIM) with a double-acting reciprocating pump (DARP). The proposed system is designed to achieve direct linear motion without needing a gearbox, thereby reducing costs and improving overall efficiency. This study presents the equivalent circuit of the LIM, including the phenomena of end effects, which increases its complexity and makes control difficult. A field-oriented control (FOC) technique is suggested to achieve better motor efficiency and dynamic performance to overcome this issue. Besides, the model of PV cells in environmental conditions, such as solar irradiance and temperature, significantly influence the I-V characteristics of PV panels. The MPPT-based P&O method was implemented to maximize their output power. The simulation results checked and validated in the Matlab/Simulink software tool demonstrate that combining LIM motors with DARP pumps offers advantages over traditional rotary motor-centrifugal pumps. This confirms that it is a beneficial solution for cost-effective, eco-friendly, and efficient irrigation.

1. INTRODUCTION

In agricultural irrigation, particularly in remote areas, most farmers rely on conventional grid electricity or diesel engines for their water-pumping systems [1]. However, diesel-based systems generate noise, pollute the air, and depend on costly fuels. Currently, water-pumping systems powered by solar energy (photovoltaic) offer significant advantages over conventional electricity- and diesel-based pumps, including cost-effectiveness and environmental benefits. Despite these advantages, it is essential to note that solar energy does not inherently operate at maximum efficiency. To ensure the optimal performance of PV systems, implementing maximum power point tracking (MPPT) strategies is essential to deliver maximum power output under varying environmental conditions [2].

On the other hand, solar water-pumping systems have often relied on rotary electric motors and centrifugal pumps [3]. To improve the reliability and affordability of water-pumping solutions, this study proposes a novel approach for enhancing the performance of a PV-powered water-pumping system by integrating a linear induction motor (LIM) with a double-acting reciprocating pump (DARP). This innovative system is designed to achieve direct linear motion without needing a gearbox, thus reducing maintenance requirements and addressing the challenges associated with converting rotational motion into linear motion. A LIM-driven reciprocating hydraulic piston pump offers several advantages over traditional centrifugal pumps, including constant flow, reduced vibration, and potentially greater efficiency, especially in off-grid or remote areas [4]. From a design perspective, the geometric configuration of the LIM is inspired by the structure of conventional rotational induction motors (RIM). Its operation is based on the interaction between the magnetic fields generated by the stator winding and the conducting layer on the surface of the secondary linear component, known as the linor. This interaction produces thrust and linear motion along the linor surface [5]. However, a significant drawback of this motor is the existence of an end-effect phenomenon that increases the complexity of the machine model. Therefore, to overcome this problem, numerous research endeavors have focused on reducing the effects of end-effect impacts and improving the control mechanisms of LIMs [6]. For control purposes, field-oriented control (FOC) is an effective method that aims to make the behavior of a LIM resemble that of a direct current (DC) motor [7]. This similarity can be achieved by aligning the motor flux with the d-axis (linor flux) and adjusting the stator currents of the d- and q-axes to control the flux and force, respectively.

Furthermore, this technique typically contributes to achieving improved efficiency, dynamic performance, and control flexibility. The main contributions of this study are as follows: in section 2, the modeling of the PV system, including the MPPT algorithm, is presented and described in detail. In section 3, An equivalent circuit of a LIM is identified by considering the end effect, and the Field-Oriented Control (FOC) scheme is modeled and presented. Section 4 details the mathematical formula for the double-acting reciprocating pump. The simulation results of the proposed approach are presented in section 5. Finally, section 6 concludes the paper.

2. MODEL OF PV CELLS AND MPPT STRATEGY

Modeling photovoltaic (PV) cells often involves using mathematical formulas to describe their electrical behavior.

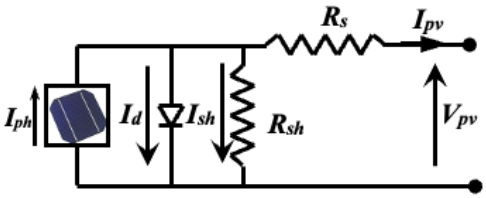

Fig. 1 – Equivalent circuit of photovoltaic cells.

One commonly used model is the single-diode model, which represents a PV cell with a simple equivalent circuit, as shown in Fig. 1.

The current-voltage (I-V) characteristics of a solar cell are described by [8]

$$I_{PV} = I_{ph} - I_D - I_{SH}, \quad (1)$$

$$I_{PV} = I_{ph} - I_S\left[\exp\left(\frac{(R_S I_{PV}+V_{PV})}{V_t}\right) - 1\right] - \left(\frac{R_S I_{PV}+V_{PV}}{R_{sh}}\right), \quad (2)$$

[1] Department of Electrical Engineering, Kasdi Merbah Ouargla University, Algeria.
[2] School for Computer Science and Advanced Techniques Epita Kremlin Bicêtre 94270, France.
E-mail: khettache.laid@univ-ouargla.dz, rezoug.redha@univ-ouargla.dz, sahraoui.lazhar@univ-ouargla.dz. akram.saadi@etu.u-pec.fr

DOI: 10.59277/RRST-EE.2025.1.1

$$V_t = \frac{N_S n k T}{q}, \tag{3}$$

$$\begin{cases} I_D = I_S\left[\exp\left(\frac{(R_S I_{PV}+V_{PV})}{V_t}\right)-1\right], \\ and \\ I_{SH} = \left(\frac{R_S I_{PV}+V_{PV}}{R_{sh}}\right), \end{cases} \tag{4}$$

$$I_{Ph} = N_p I_{Ph-cell}, \qquad I_S = N_p I_{S-cell}. \tag{5}$$

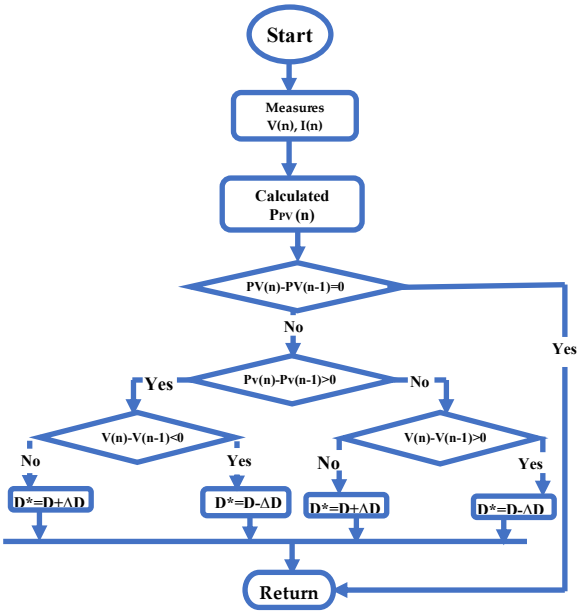

Fig. 2 – Flowchart of P&O MPPT algorithm [10].

The implementation of MPPT strategies is an essential part of maximizing the output power of PV systems. This section's flowchart in Fig. 2 illustrates the proposed perturb-and-observe (P&O) algorithm [9].

3. MOTOR AND CONTROL STRATEGY

3.1 MODEL OF LINEAR INDUCTION MOTOR

The dynamic model of the linear induction motor was investigated through the d-q model of the equivalent electrical circuit, considering the phenomenon of the end effect. Ducan [11] and Gieras et al. [12] developed equivalent circuits by superposing the synchronous and pulsating waves caused by the end effect.

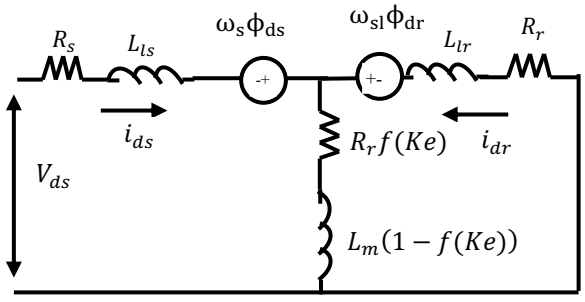

(a) d-axis equivalent circuit.

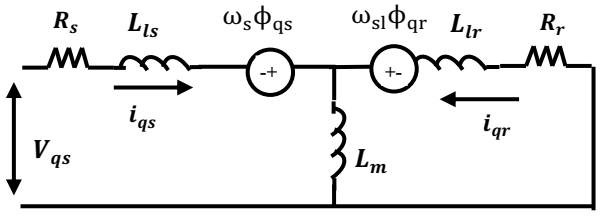

(b) q-axis equivalent circuit.

Fig. 3 – LIM equivalent electrical circuit considering end-effects.

As depicted in Fig. 3, the equivalent circuit of the LIM can be divided into two parts. The first part, shown in Fig. 3(a), is influenced by the end effect, particularly along the d-axis, where the parameters vary accordingly. The second part, illustrated in Fig. 3(b), remains unaffected by this phenomenon, resembling the q-axis equivalent circuit of the induction motor. Here, Ψ, L, and R represent flux, inductance, and resistance. The subscripts d and q denote the components of each physical quantity in the d- and q-axis systems, while s and r refer to primary and secondary aspects. Additionally, ω_s and ω_{sl}, signifying the primary electrical angular frequency and slip angular frequency, respectively [13].

In [11,14], *Ke* is an important parameter that is used to express the end-effects phenomenon:

$$Ke = \frac{DR_r}{(L_m+L_{lr})v}. \tag{6}$$

The three-phase magnetizing inductance varying with *Ke* is defined as

$$\hat{L}_m = L_m[1-f(K_e)]. \tag{7}$$

where:

$$f(K_e) = \frac{1-e^{-K_e}}{K_e}. \tag{8}$$

when considering the eddy current losses, a resistance emerges in the transverse branch, denoted as $\hat{R}_r$, and is defined as:

$$\hat{R}_r = R_r f(K_e). \tag{9}$$

For the circuits, the voltage and linkage flux equations of the LIM in the d-q reference frame are expressed as follows:

$$\begin{cases} V_{ds} = R_s i_{ds} + R_r f(K_e)(i_{ds}+i_{dr}) + \frac{d\phi_{ds}}{dt} - \omega_s\phi_{qs}, \\ V_{qs} = R_s i_{qs} + \frac{d\phi_{qs}}{dt} + \omega_s\phi_{ds}, \\ 0 = R_r i_{dr} + R_r f(K_e)(i_{ds}+i_{dr}) + \frac{d\phi_{dr}}{dt} - \omega_{sl}\phi_{qr}, \\ 0 = R_r i_{qr} + \frac{d\phi_{qr}}{dt} + \omega_{sl}\phi_{dr}, \end{cases} \tag{10}$$

$$\begin{cases} \phi_{ds} = L_{ls} i_{ds} + L_m\big(1-f(Ke)\big)(i_{ds}+i_{dr}), \\ \phi_{qs} = L_{ls} i_{qs} + L_m\big(i_{qs}+i_{qr}\big), \\ \phi_{dr} = L_{lr} i_{dr} + L_m\big(1-f(Ke)\big)(i_{ds}+i_{dr}), \\ \phi_{qr} = L_{lr} i_{qr} + L_m\big(i_{qs}+i_{qr}\big). \end{cases} \tag{11}$$

The primary angular frequency was determined by combining the linor angular speed with the slip frequency. This relationship is defined as

$$\omega_s = \omega_{sl} + \omega_r \tag{12}$$

Additionally, the conversion of the LIM's angular speed to linear speed is represented as:

$$v = \frac{\tau_p}{\pi}\omega_r \tag{13}$$

In this study, the linear motor was directly connected to the pump, and the gearbox was neglected. The dynamic equation of the linear induction motor (LIM) is [15]

$$M\frac{d}{dt}v + Bv = F_e - F_L, \tag{14}$$

where *M* is the mass of the moving parts of the motor and pump, and *B* is the damping coefficient.

The electromagnetic force F_e applied by the motor is

defined as:

$$F_e = \frac{3\pi}{2\tau_p}\frac{p}{2}\left(\phi_{ds} i_{qs} - \phi_{qs} i_{ds}\right), \quad (15)$$

and

$$F_e = \frac{3\pi}{2\tau_p}\frac{p}{2}\frac{L_m(1-f(K_e))}{L_r - L_m f(K_e)}\left(\phi_{dr} i_{qs} - \phi_{qr} i_{ds}\right) = M\frac{d}{dt}v + Bv + F_L. \quad (16)$$

Moreover F_L is the load force caused by the weight of the lifted water.

$$F_L = F_{pump}. \quad (17)$$

2.1 FIELD-ORIENTED VECTOR CONTROL

FOC has become more widely used in modern motor control due to its efficacy in achieving high efficiency and dynamic performance. Like the control principles applied in separately excited DC motors, FOC aims to decouple torque and flux control within the motor system. By aligning the d-axis with the linor flux, the control system can independently regulate the torque-producing current (Iq) along the d-axis and the magnetizing current (Id) along the q-axis. Figure 4 illustrates the dynamic model of FOC applied to the LIM, considering the end effect in the synchronously rotating reference frame [16].

Under rotor flux orientation conditions, the linor flux equations can be given as follows:

$$\begin{cases} \phi_{qr} = 0, \\ \phi_{dr} = \phi_r = constant. \end{cases} \quad (18)$$

Substituting eq (18) into the linor linkage flux eq. (10), the linor currents are derived as in eq. (19) and (20)

$$i_{dr} = \frac{\phi_r - \hat{L}_m i_{ds}}{L_r}, \quad (19)$$

with $L_r = L_{lr} + L_m[1 - f(K_e)]$,

$$i_{qr} = \frac{-L_m . i_{qs}}{L_{lr} + L_m}. \quad (20)$$

where: L_r is the secondary inductance, L_{lr} the secondary leakage inductance, and L_m the magnetizing inductance. By employing eq. (18) and (20) within the stator voltage eq. (10), the decoupling current and voltage compensation can be expressed as

$$\begin{cases} V_{ds} = \left(R_s + \hat{R}_r - \frac{\hat{R}_r . \hat{L}_m}{L_r}\right) i_{ds} + \frac{\hat{R}_r}{L_r}\phi_r + \sigma L_s \frac{\mathrm{d}i_{ds}}{\mathrm{d}t} - \omega_s \sigma' i_{ds}, \\ V_{qs} = R_s i_{qs} + \sigma' \frac{\mathrm{d}i_{qs}}{\mathrm{d}t} + \omega_s \sigma L_s i_{ds} + \omega_s \frac{\hat{L}_m}{L_r}\phi_r. \end{cases} \quad (21)$$

As illustrated in eq. (22), the stator voltage components are coupled by the d- and q-back electromotive force given by

$$\begin{cases} E_d = -\frac{\hat{R}_r}{L_r}\phi_r + \omega_s \sigma' i_{ds}, \\ E_q = -\omega_s \sigma L_s i_{ds} - \omega_s \frac{\hat{L}_m}{L_r}\phi_r. \end{cases} \quad (22)$$

Finally, the feed-forward decoupling method [17] is applied to obtain the linear terms as follows:

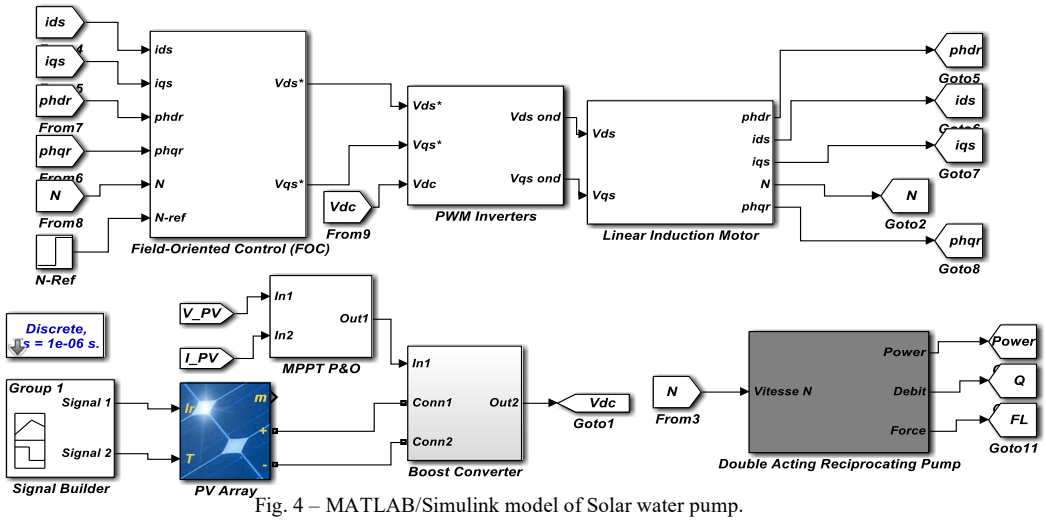

Fig. 4 – MATLAB/Simulink model of Solar water pump.

$$\begin{cases} V'_{ds} = \left(R_s + \hat{R}_r - \frac{\hat{R}_r . \hat{L}_m}{L_r}\right) i_{ds} + \sigma L_s \frac{\mathrm{d}i_{ds}}{\mathrm{d}t}, \\ V'_{qs} = R_s i_{qs} + \sigma' \frac{\mathrm{d}i_{qs}}{\mathrm{d}t}, \end{cases} \quad (23)$$

$$L_s = L_{ls} +, , \quad (24)$$

$$\begin{cases} \sigma = 1 - \frac{\hat{L}_m^2}{L_s L_m}, \\ \sigma' = (L_{ls} + L_m) - \frac{L_m^2}{(L_{lr} + L_m)}. \end{cases} \quad (25)$$

In a more detailed model, the thrust force is represented in the linor flux-oriented reference frame as follows.

$$F_e^* = K_f, , \quad (26)$$

$$K_f = \frac{3\pi}{2\tau_p}\frac{p}{2}\frac{L_m(1-f(Q))}{L_r - L_m f(Q)}\phi_{dr}^*, \quad (27)$$

$$i_{qs}^* = \frac{4\tau_p}{3\pi p}\frac{L_r - L_m f(Q)}{L_m(1-f(Q))}\frac{F_e^*}{\phi_{dr}^*}. \quad (28)$$

3. DOUBLE ACTING RECIPROCATING PUMP

Water exerts force on both sides of the piston for this type of pump. Consequently, this design necessitates using two suction pipes and two delivery pipes. This configuration required two suction valves (S1 and S2) and two delivery valves (D1 and D2), illustrated in Fig. 5 [18].

During the process of coupling the motor to the pump, the displacement of the actuator is equal to the downward and upward strokes of the piston. Consequently, a power converter must sequentially energize the phase windings of the motor and reverse the sequence each time the end positions of the actuator are reached [19].

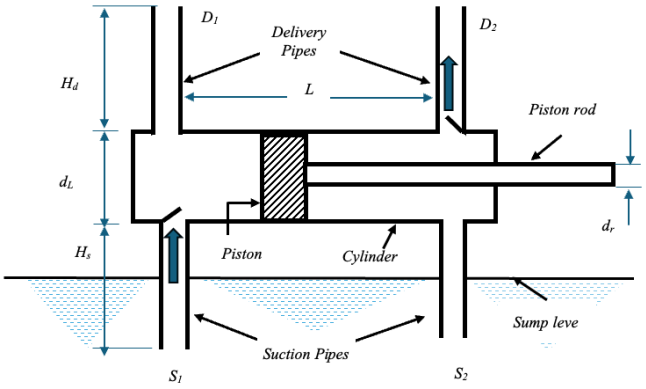

Fig. 5 – Main parts of double-acting reciprocating pump.

The power requirement of a double-acting reciprocating pump can be estimated using the following formula:

$$P = \frac{QH\rho g}{\eta}, \tag{29}$$

$$H = H_s + H_d, \tag{30}$$

where P is the power (W) required by the pump, H is the total head (m), ρ is the density of the fluid being pumped (kg/m^3), g is the acceleration due to gravity (approximately 9.81 m/s), and η is the overall efficiency of the pump and motor systems (expressed as a decimal).

This formula estimates the power required for the pump under steady-state conditions, assuming an ideal behavior.

The capacity or flow rate (Q) of a double-acting reciprocating pump can be calculated using [20]:

$$Q = \frac{2ALN}{60}. \tag{31}$$

4. SIMULATION RESULTS

This section conducts a simulation using MATLAB/Simulink to demonstrate the performance of the proposed design system. We employed the **China Sunergy Nanjing SST235-60P with eight series modules, one parallel string (**see Table 3 in the appendix**),** and the P&O MPPT algorithm to verify and validate the proposed approach. Furthermore, the parameters of the LIM used in this research are summarized in Table 1.

Table 1

Linear induction motor parameters

Parameters	Values
Primary resistance – $\boldsymbol{R_s}$	1.25 Ω
Linor resistance – $\boldsymbol{R_r}$	2.7 Ω
Primary leakage inductance – $\boldsymbol{L_{ls}}$	40.1 mH
Linor leakage inductance – $\boldsymbol{L_{lr}}$	33.1 mH
Magnetizing inductance – $\boldsymbol{L_m}$	32.6 mH
Pole pitch – $\boldsymbol{\tau_p}$	0.0641 m
Primary length – D	0.286 m
Mass of the LIM – M	8 kg
Number of pole pairs – p	4

The I-V and P-V characteristics of the PV module are shown in Fig. 6 (a and b), with the different solar irradiance values used between 700 W/m and 1000 W/m. Then, the illumination profile is illustrated in Fig. 8(c), with the temperature retained at a fixed value of 25 °C.

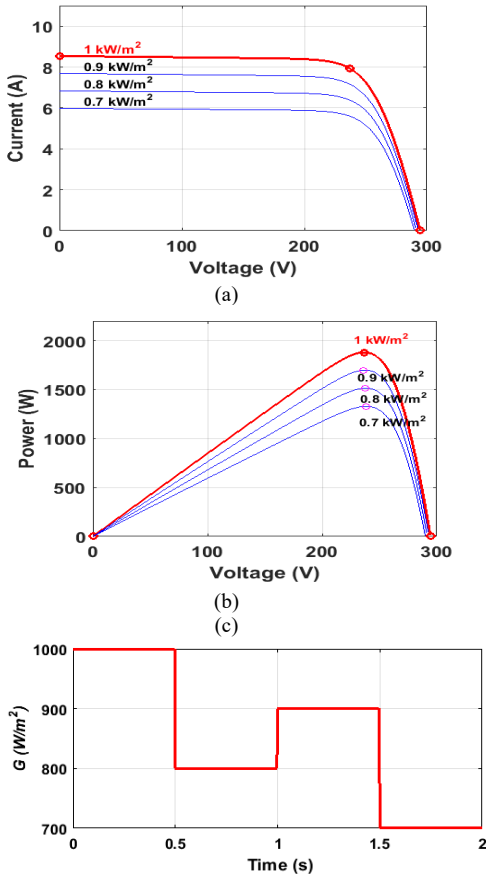

Fig. 6 – (I–V) and (P–V) characteristics of the PV array under different solar irradiance.

The output of the PV-array module is shown in Fig. 7. the PV output voltage is obtained near 250 V, and the PV output current is changed between 7.23 A to 5.024 A due to variations in solar irradiance G.

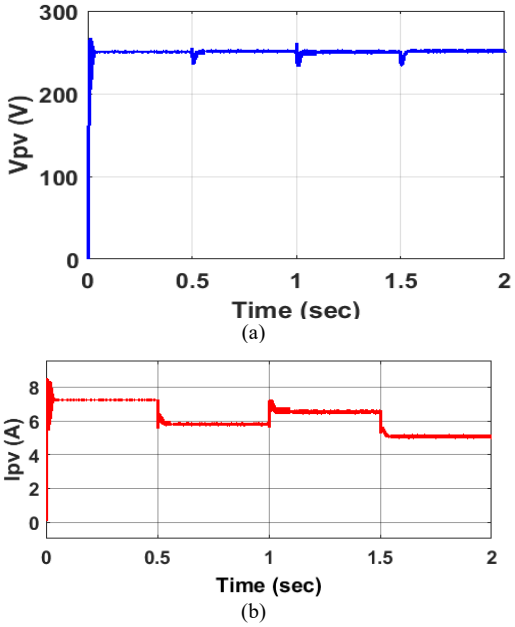

Fig. 7 – PV output voltage and current under varying solar irradiance.

To demonstrate the effectiveness of the proposed FOC control method, the motor was run with a 3 m/s reference speed and 0.4 Wb reference flux, and the external load force was applied, which signified that the motor is coupled

to the pump (load pump) see Fig. 8.

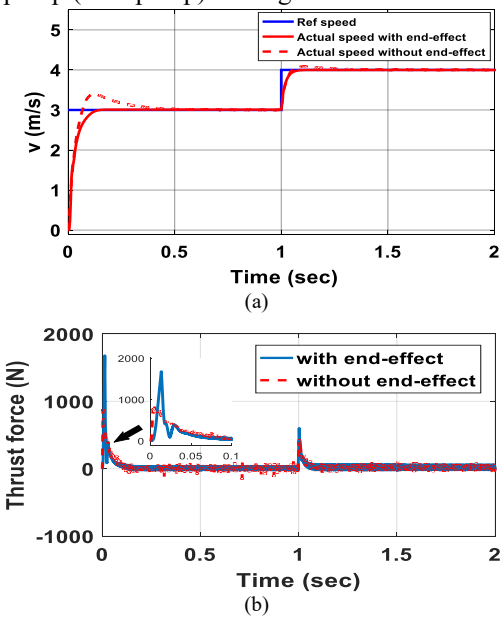

Fig. 8 – Speed and thrust force responses under reference speed variation between 3 m/s and 4 m/s.

Figure 8 (a) confirms that the performance of the speed controller was tested by applying a significant change in the reference speed from 3 m/s to 4 m/s at t =1 s. The actual motor speed (red line) almost tracks the reference speed (blue line) for both values, which indicates effective speed control.

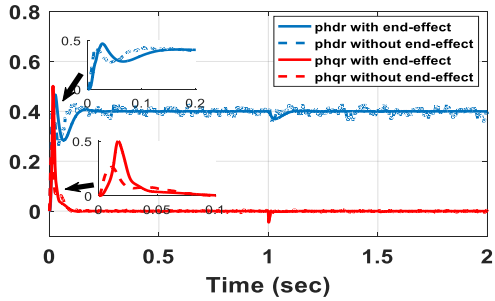

Fig. 9 – Direct and Quadrature linor flux responses.

In addition, the components of linor flux are depicted in Fig. 9. It is noted that decoupling between the direct and quadrature linor flux is performed correctly since ϕ_{dr} is not affected significantly (ϕ_{dr} is kept constant at the reference value ϕ_{dr} = 0.4 Wb). At the same time, ϕ_{qr} is maintained at zero (ϕ_{qr} = 0 Wb). When the speed reference changes, remarkable peaks are observed at t = 1 sec.

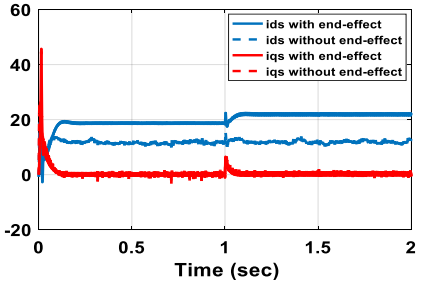

Fig. 10 – Direct and quadrature stator current responses.

On the other hand, Fig. 10 illustrates the stator current components i_d and i_q response obtained by minimizing the error between actual and reference values of force and flux. As shown, when the d-axis current changes (i_{ds} = 18.75 A to 21.94 A) due to a change in speed reference, the q-axis current is only slightly disturbed and then quickly recovers to its commanded value i_{qs} = 0.41 A, as determined accordingly to reference force eq. (28). So, the decoupling between the direct and quadrature stator current was successfully achieved.

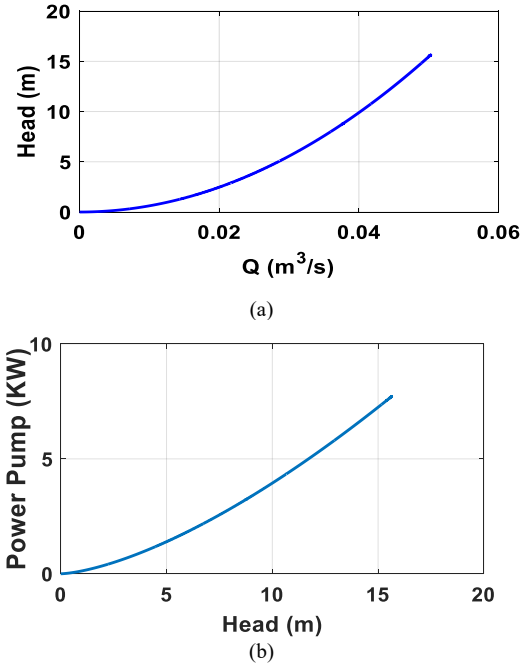

Fig. 11 – Pump performance curves: (a) Head vs. Flow, (b) Power vs. Head.

Furthermore, for different Head (H) values, Fig. 11 demonstrates the flow rate (Q) and pump power increases. To assess the performance of the proposed design, Table 2 recapitulates the performance of a double action reciprocating pump and a linear induction motor in terms of Q.

Table 2

Performance comparison of the proposed PV-water system-based DAR pump and LIM with the conventional rotary motor-centrifuge pump.

References	Speed	flow rate Q (m^3/s)
[21]	2534 (RPM)	3.362 (L/s)
	2711 (RPM)	4.135 (L/s)
[22]	120 (rad/s)	0.0078 (m^3/s)
	150 (rad/s)	0.009 (m^3/s)
This work	3 (m/s)	0.0377 (m^3/s)
	4 (m/s)	0.05 (m^3/s)

4. CONCLUSION

This paper has demonstrated the application of a linear induction motor with a double-action pump (DAR) to enhance photovoltaic-water pumping systems. Field-oriented control is introduced to regulate the dynamic model (Motor-pump). Simulation results show that the proposed FOC technique achieves accurate speed tracking with minimal error and short response time across different speed reference values, enhancing decoupling between force and flux. A comparative analysis of both models, distinguished by the exclusion or inclusion of the end effect, revealed significant improvements, which are summarized as follows:

- Overshoot reduction: from 13 % to 0 %.
- The settling time decreased from 0.56 to 0.14 s.
- Increase in current (ids): from 11.91 A to 18.75 A.

- The model with the end effect demonstrated greater efficiency, providing more stable control of key variables such as speed, thrust force, current, and magnetic flux.

The successful implementation of this approach offers a sustainable and cost-effective solution for agricultural applications, including high system reliability and a low-cost implementation process.

CREDIT AUTHORSHIP CONTRIBUTION

Laid Khettache: presented idea.
Mohamed Redha Rezoug: Theory and performed simulation.
Akram Saadi: Results analysis and data.
Lazhar Sahraoui: Designed the methodology.

Received on 20 March 2024

NOMENCLATURE

V_{ds}, V_{qs}: primary voltages in the d-q axes (V).
i_{ds}, i_{qs}: d-q axes primary currents (A).
i_{dr}, i_{qr}: d-q axes linor currents (A).
ϕ_{ds}, ϕ_{qs}: d-q axes primary flux linkages (Wb).
ϕ_{dr}, ϕ_{qr}: d-q axes linor flux linkages (Wb).
L_s, L_r: primary and linor self-inductances (H).
R_s, R_r: primary and linor resistances (Ω).
Ke: factor associated with the length of linor.
F_e: Electromagnetic force (thrust force).
τ_p: pole pitch (m).
D: length of the linor (m)
p: number of poles.
v: velocity (m/s).
ω_s: primary angular velocity (rad/sec).
ω_r: linor angular velocity (rad/sec).
ω_{sl}: slip frequency (rad/sec).
Q: flow rate (m3/s).
L: stroke length (m).
N: pump speed (rpm).
σ, σ′: leakage coefficients associated with cases with and without end-effect.
A: piston area (m^2).
I_{PV}: output current of the solar cell.
I_{ph}: photocurrent proportional to isolation.
I_0: reverse saturation current of the diode.
V_{PV}: output voltage of the solar cell.
n: ideality factor of the diode.
q: electron charge (approximately 1.602×10−19 °C).
K: Boltzmann constant (approximately 1.381×10−23 J/K).
T: junction temperature (Kelvin).
R_s, R_{sh}: series, and shunt resistance of the solar cell (Ω).

APPENDIX

Table 3
Manufacturer Specifications for a PV Module (China Sunergy (Nanjing) SST235-60P; 8 series modules; 1 parallel strings).

Pv Parameters	Value
Maximum Power	235.024 W
Cells per module (Ncell)	60
Open circuit voltage V_{oc}	36.8 V
Short-circuit current I_{sc}	8.54 A
Voltage at maximum power point V_{mp}	29.6 V
Current at maximum power point I_{mp}	7.94 A
Shunt resistance *R*sh	194.48 Ω

REFERENCE

1. H.K.V. Gadiraju, V.R. Barry, R.K. Jain, *Improved performance of PV water pumping system using dynamic reconfiguration algorithm under partial shading conditions*, CPSS Transactions on Power Electronics and Applications, **7**, *2*, pp. 206–215 (2022).
2. L. Gevorkov, J.L. Domínguez-García, L.T. Romero. *Review on solar photovoltaic-powered pumping systems*, Energies, **16,** *1*, pp.94 (2023).
3. R. Kahani, M. Jamil. M.T. Iqbal. *An improved perturb and observed maximum power point tracking algorithm for photovoltaic power systems*, Journal of Modern Power Systems and Clean Energy, **11**, *4*, pp. 1165–1175 (2023).
4. H. Yeqing, N. Songlin, M. Kai, L. Fan, L. Lei, *Static stress and modal analysis of water hydraulic reciprocating piston pump driven by the linear motor*, International Conference on Fluid Power and Mechatronics (FPM), Harbin, China, pp. 914–917 (2015).
5. R. Rajan, L.A.R. Krishna, S. Sreeja, *Mathematical modelling and analysis of linear induction motor*, IEEE International Power and Renewable Energy Conference (IPRECON), Kollam, India, pp. 1–6 (2022).
6. A. Mousaei, M.B. Bannae Sharifian, N. Rostami, *An improved predictive current control strategy of linear induction motor based on ultra-local model and extended state observer*, 13th Power Electronics, Drive Systems and Technologies Conference (PEDSTC), Tehran, Iran, Islamic Republic of, pp. 12–18 (2022).
7. P. Marcello, *Direct field-oriented control of linear induction motors*. Electric Power Systems Research, **89**, pp. 11–22 (2021).
8. M.R. Rezoug, R. Chenni, D. Taibi, *Fuzzy logic-based perturb and observe algorithm with variable step of a reference voltage for solar permanent magnet synchronous motor drive system fed by direct-connected photovoltaic array*, Energies, **11**, *2*, pp. 462 (2018).
9. N. Kacimi, A. Idir, S. Grouni, MS. Boucherit, *A new combined method for tracking the global maximum power point of photovoltaic systems,* RRST-EE, **67**, *3*, pp. 349–54 (2022).
10. S. Samah, M. Birane, K. Benmouiza, *A comparative analysis of boost converter topologies for photovoltaic systems using MPPT (Po) and Beta methods under partial shading*, RRST-EE, **68**, *4*, pp. 375–380 (2023).
11. J. Duncan, *Linear induction motor-equivalent-circuit model,* IEE Proc. B, Electron. Power Appl., **130**, *1*, pp. 51–57 (1983).
12. J.F. Gieras, G.E. Dawson, A.R. Eastham, *A new longitudinal end effect factor for linear induction motor,* IEEE Transactions on energy conversion, **EC-2**, *1*, pp. 152–159 (1987).
13. L. Khettache, R. Abdessemed, *A new speed control approach of linear induction motor based on robust RST controller and model reference adaptive system estimator,* International Journal of Engineering, **36**, *4*, pp. 630–639 (2023).
14. L. Zhang, H. Obeid, S. Laghrouche, M. Cirrincione, *Second order sliding mode observer of linear induction motor*, IET Electric Power Applications, **13**, *1*, pp. 38–47 (2019).
15. H.A. Hussain, H.A. Toliyat, *A fault monitoring system for a reciprocating pump driven by a linear motor for oil pumping systems*, IEEE Energy Conversion Congress and Exposition (ECCE), Cincinnati, OH, USA, pp. 4338–4344 (2017).
16. K. Wang, Y. Li, Q. Ge, L. Shi, *An improved indirect field-oriented control scheme for linear induction motor traction drives,* IEEE-Transactions on Industrial Electronics, **65**, *12*, pp. 9928–9937 (2018).
17. D.B. Jani, C. Chetan, J. Chauhan, Da. Baria, U. Barjod, J. Bangadiya, *Performance investigation on double acting reciprocating pump*, Applied Energy. **6**, *4* pp. 14–17 (2019).
18. G. Boyun, X. Liu, X. Tan, *Transportation systems*, Petroleum Production Engineering, Gulf Professional Publishing, pp. 275–325 (2017).
19. C.F. Lieu, W.K. Chan, K.T. Ooi, *Experimental investigation of the reciprocating ball pump (RBP)*, Medical Engineering & Physics, **34**, pp. 1101– 1108 (2012).
20. J. Pei, C. He, M. Lv, X. Huang, K. Shen, K. Bi, *The valve motion characteristics of a reciprocating pump*, Mech. Syst. Signal Process., **66–67**, pp. 657–664 (2016).
21. S. Pant, R.P. Saini, *Solar water pumping system modelling and analysis using MATLAB/Simulink*. IEEE Students Conference on Engineering & Systems (SCES), Prayagraj, India, pp. 1–6 (2020).
22. M. Errouha, S. Motahhir, Q. Combe, et al., *Intelligent control of induction motor for photovoltaic water pumping system*.SN Appl. Sci., **3**, *777* (2021).